Rattle-Structured Upconversion Nanoparticles for Near-IR-Induced Suppression of Alzheimer's β-Amyloid Aggregation

*Sukeun Kuk, Byung Il Lee, Joon Seok Lee, and Chan Beum Park**

Alzheimer's disease (AD) is the most prevalent neurodegenerative disorder characterized by a progressive impairment of the patient's cognitive and memory ability. The excess production and aggregation of β-amyloid (Aβ) peptide in the brain is recognized as a representative pathological hallmark of AD.[1] Though the role of Aβ in normal physiology and an exact mechanism of its aggregation are not clearly elucidated yet,[2] abnormal assembly of monomeric Aβ composed of 42 or 40 amino acids into oligomers (or fibrils) is considered as an initiation of AD pathogenesis.[3] Accordingly, numerous efforts have been made to develop therapeutic agents that can prevent the release or aggregation of Aβ peptides.[4–7] In addition to the typical chemotherapeutic approach, a few photosensitizing chemicals have been reported recently as a visible (or UV) light-responsive inhibitor of Aβ fibrillogenesis.[8–11] Also, photoresponsive nanomaterials have been explored as potential inhibitors of Aβ aggregation.[12–14] For example, Chung et al. showed that photoexcited graphitic carbon nitride nanosheets produce photoexcited electrons that generate oxidative stress to block Aβ aggregation.[13] In addition, photochemical suppression of Aβ aggregation by polyoxometalatates was reported recently.[14]

The utilization of light in medical therapy attracted substantial interest in treating local diseases, such as cancer, because of its noninvasiveness and reduced side effects compared to surgery and chemotherapy.[15] In the photodynamic therapy (PDT), however, visible (or UV) light-activated photosensitizers can pose a significant problem because of a limited penetration depth of UV–visible light in biological tissues. In contrast, near-infrared (NIR) light shows highly improved tissue penetration depth because the absorbance of most tissues and biological fluids reaches the minimum in the wavelength range of 700–1100 nm. In this context, the materials that can effectively utilize the energy from NIR light are attractive for therapeutic applications. For example, upconversion nanoparticles (UCNPs), which have an ability to convert NIR light into short wavelength radiation (e.g., visible or UV light) via two photons or a multiphoton mechanism, have gained considerable attention recently.[16,17] Different nanocomposites composed of UCNPs and photosensitizers have been studied for bioimaging, biosensing, and photodynamic therapy.[18–22] Moreover, a recent study proposed a delivery of UCNPs across the blood–brain barrier (BBB) via a functionalization of ligands on their surface.[23]

Here, we report NIR-light-induced suppression of Aβ aggregation using UCNPs. We synthesized rattle-structured organosilica (ROS)-shell-coated, Yb/Er-co-doped $NaYF_4$ nanoparticles as an energy transducer to activate visible light-absorbing photosensitizers that suppress Aβ aggregation upon excitation, as depicted in **Scheme 1**. While the upconverting nanocomposites with the core–shell design have been studied in various fields including PDT[24,25] and artificial photosynthesis,[26] the application of the nanostructure to the treatment of neurodegenerative disease has not been investigated yet. In addition, The ROS-shell-coated UCNPs exhibit a high efficiency of energy transfer from UCNPs to photosensitizers because of an interior cavity between UCNP core and porous organosilica shell, which provides high loading capacity, short distance between UCNPs and photosensitizers, and reduced self-aggregation of photosensitizers.[27] Among various UCNPs, $NaYF_4$ nanoparticles doped with lanthanide ions (Ln^{3+}, such as Yb^{3+}, Er^{3+}, and Tm^{3+}) possess high NIR-to-visible upconversion efficiency.[26] We chose rose bengal (RB) as a model photosensitizer to be loaded to the ROS-shell-coated UCNPs, because its absorbance overlaps considerably with the green upconversion emission of $NaYF_4$:Yb,Er.

We synthesized monodispersed $NaYF_4$:Yb,Er UCNPs by thermal decomposition method. They exhibited a highly crystalline hexagonal phase with ≈50 nm diameter, according to our analyses using transmission electron microscope (TEM) and X-ray diffraction (XRD) (**Figure 1**a and Figure S1, Supporting Information). After the coating of thin pure-silica shell and organosilica layer on the UCNPs with ≈22.5 nm thickness (Figure 1b), we created a porous ROS shell by surface-protected, hot-water etching process (Figure 1c). Average internal cavity diameter of the UCNPs with the ROS shell (UCNP@ROS) was ≈65 nm and the

S. Kuk, B. I. Lee, Dr. J. S. Lee, Prof. C. B. Park
Department of Materials Science and Engineering
Korea Advanced Institute of Science
and Technology (KAIST)
291 Daehak-ro, Yuseong-gu
Daejeon 34141, Republic of Korea
E-mail: parkcb@kaist.ac.kr

DOI: 10.1002/smll.201603139

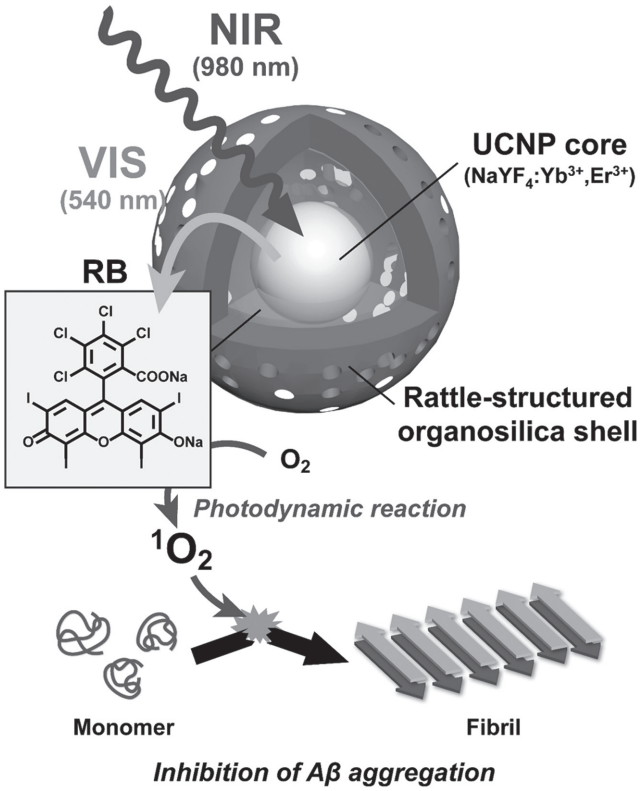

Scheme 1. Schematic illustration of β-amyloid aggregation inhibition by near-infrared (NIR)-mediated rattle structured upconversion nanoparticles loaded with rose bengal (RB). Under NIR light (980 nm) illumination, rattle-structured upconversion nanoparticles ($NaYF_4$:Yb,Er) emit visible light (540 and 660 nm) that can be absorbed by loaded RB. Photoexcited RB generates singlet oxygen ($^1O_2$) through photodynamic reaction, which can suppress the aggregation of β-amyloid.

mean gap between the shell and the core UCNP was about 7.5 nm. The mean gap was estimated from the average difference between a diameter of the UCNP core and the etched internal cavity diameter of ROS shell. The ROS shell exhibited a narrow pore size distribution of ≈4 nm of mean value (Figure 1d) with surface area of 194.8 m^2 g^{-1} and pore volume of 0.34 cm^2 g^{-1}. We further analyzed UCNP@ROS by elemental mapping using scanning transmission electron microscope (STEM) (Figure 1e). Through Yb elemental distribution, we observed that $NaYF_4$:Yb,Er UCNP was located well inside the ROS shell (Figure S2, Supporting Information). Furthermore, C, O, Si, and N elemental maps indicated that organosilica shell was well synthesized with equally distributed phenylene and amine group. The ^{13}C and ^{29}Si cross-polarization magnetic angle spinning (CP-MAS) nuclear magnetic resonance (NMR) spectra of UCNP@ROS identified the ROS shell as a phenylene-bridged polysilsequioxane with amine organic moieties (Figure 1f,g). Fourier transform infrared spectrophotometer (FTIR) spectroscopy and zeta potential analysis also supported the existence of phenylene and amine groups in the ROS shell (Figures S3 and S4, Supporting Information).

We observed that UCNP@ROS emitted upconverting visible fluorescence at 522 nm ($^2H_{11/2}\rightarrow{}^4I_{15/2}$), 542 nm ($^4S_{3/2}\rightarrow{}^4I_{15/2}$), and 656 nm ($^4F_{9/2}\rightarrow{}^4I_{15/2}$) under 980 nm NIR irradiation. The major peak of UCNP@ROS green emission matched well with the absorbance spectrum of free RB, thus making the energy transfer between UCNPs and RB possible through Förster resonance energy transfer (FRET) (Figure S5, Supporting Information). To load a photosensitizer in the ROS structure, we soaked UCNP@ROS in RB-containing dimethylforamide (DMF) solution for 1 d with vigorous stirring. As shown in **Figure 2**a, the amount of embodied RB in the ROS shell increased with the increasing concentration of RB in the solution and reached loading capacity saturation at 5%, which is 2.5-folds higher than that of mesoporous-silica-shell coated UCNP (UCNP@MS). We confirmed that the loaded RB in the UCNP@ROS did not leak over 7 d (Figure S6, Supporting Information). This high loading capacity is attributed to internal cavities in UCNP@ROS and to interactions between RB and amine functional moiety and the phenylene group in the ROS shell. Positively charged amine functional moiety induced electrostatic attraction with anionic part of RB and phenylene-group-led hydrophobic and π–π stacking interactions with aromatic ring in RB. Zeta potential decrease after RB loading proved the electrostatic attraction of amine functional group (Figure S7a, Supporting Information). Furthermore, we observed that hydrophobic interaction and π–π stacking interaction of phenylene group inhibit self-aggregation of RB molecules. According to the literature,[28] h-aggregation, which refers to the face-to-face stacking of molecules, of RB induces self-quenching, diminishing the yield of singlet oxygen ($^1O_2$) generation. In aqueous solutions, RB's h-aggregation to dimers or oligomers exhibits a blue shift (or hypsochromic shift) in UV–vis absorption spectra. As shown in Figure 2b, we observed a suppressed blue shift of RB in UCNP@ROS in absorption spectrum compared to that of the UCNP@MS, which indicates a positive effect of the ROS shell on RB disaggregation offering more efficient energy transfer.

We investigated the energy transfer from UCNP@ROS to RB according to fluorescence spectra and UC luminescence (UCL) lifetime decay curves. Figure 2c shows that the green emission bands at 522 and 542 nm of UCNP@ROS were drastically quenched after RB loading, while the emission at 656 nm was not. The efficiency of energy transfer was calculated to be 97.8%, which is defined as $(I_0–I_1)/I_0$ where I_0 and I_1 are the integrated emission of green UC emission bands of UCNP@ROS in the absence and presence of RB, respectively.[27] Further energy transfer analysis was carried out by measuring lifetime of upconversion luminescence. The average lifetime decay (0.10 ms) of RB-loaded UCNP@ROS at 542 nm was shorter compared to that (0.14 ms) of UCNP@ROS (Figure 2d), which indicates efficient energy transfer from UCNP to RB. On the other hand, the monitored lifetime decay at 656 nm displayed scant change (0.31–0.30 ms, Figure S8, Supporting Information). The difference in the lifetime decrease between green emission spectra and red emission spectra implied selective energy transfer due to RB absorbance spectra. The high FRET efficiency from UCNP@ROS to RB is attributed to the high loading capacity as well as the disaggregation of RB. The direct contact of UCNP and RB within the cavity should decrease the nonradiative excitation energy loss of UCNP, an energy

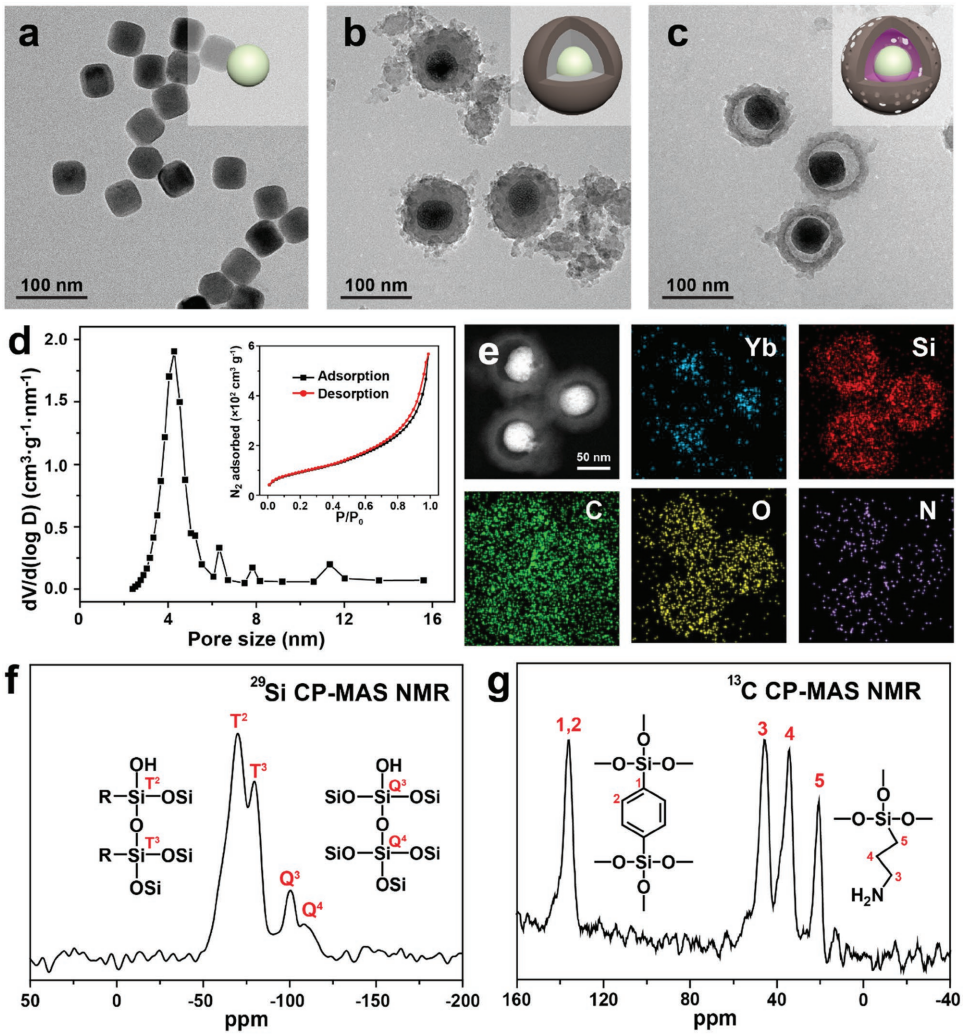

Figure 1. TEM images of a) $NaYF_4$:Yb,Er (UCNP), b) UCNP@OS, and c) UCNP@ROS. The insets are schematic descriptions of nanoparticles at each step. Scale bars: 100 nm. d) Pore size distribution of UCNP@ROS determined from N_2 adsorption–desorption analysis (Inset: N_2 adsorption–desorption isotherm). e) STEM image of UCNP@ROS and elemental mapping of Yb, Er, Si, O, and N elements. Scale bar: 50 nm. f) ^{29}Si CP-MAS NMR spectra of UCNP@ROS. Chemical shifts of tertiary silicon (T^2 at –69.9 ppm, T^3 at –79.7 ppm) and quaternary silicon (Q^3 at –100.3 ppm, Q^4 at –108.0 ppm) indicate mesoporous silica framework in ROS shell. g) ^{13}C CP-MAS NMR spectra of UCNP@ROS. A single peak at 134 ppm, and three peaks observed at 45.8, 34.1, and 20.5 ppm correspond to phenylene bridge and aminopropyl organic moieties, respectively.

donor, and enhanced the energy transfer to disaggregated RB, an energy acceptor.

We employed multiple photochemical analyses to monitor the NIR-induced inhibitory effect of RB-loaded UCNP@ROS on Aβ aggregation. Circular dichroism (CD) spectrum of nontreated Aβ shows a typical profile of β-sheet-rich proteins after the incubation for 24 h, which includes a positive band at 195 nm and a negative band at 216 nm, indicating the assembly of Aβ monomers into fibrils.[29] Neither NIR-light itself nor RB/UCNP@ROS (without light) affected Aβ aggregation according to the CD result (**Figure 3**a). Only when Aβ monomers were incubated with RB/UCNP@ROS under NIR light illumination did the representative peaks of β-sheet structure disappear, which indicates that Aβ aggregation was hindered by NIR-sensitized RB/UCNP@ROS. Both atomic force microscopy (AFM) and native gel electrophoresis results further support the inhibitory effect; high density of amyloid fibrils was observed in the AFM images of nontreated Aβ solution under dark or NIR light (Figure 3c,d), showing negligible effect of NIR light itself on Aβ aggregation. While numerous short fibrils were concentrated around the nanoparticles incubated with Aβ monomers under dark (Figure 3e), only a few fibrils and nanoparticle clusters were found when incubated under NIR light, which shows that Aβ fibrillogenesis was significantly precluded RB/UCNP@ROS under NIR light illumination. According to native gel electrophoresis result (Figure S9, Supporting Information), a high-intensity band of a molecular weight of 4.5 kDa corresponding to Aβ monomer was observed only when Aβ was incubated with RB/UCNP@ROS under NIR light illumination. The two bands near 15 kDa correspond to the trimer (13.5 kDa) and tetramer (18 kDa) of Aβ peptide, which were appeared due to the increased monomeric contents. The increased intensity of Aβ monomer band implies a blocked conversion of monomers into aggregates by NIR light-sensitized RB/UCNP@ROS.

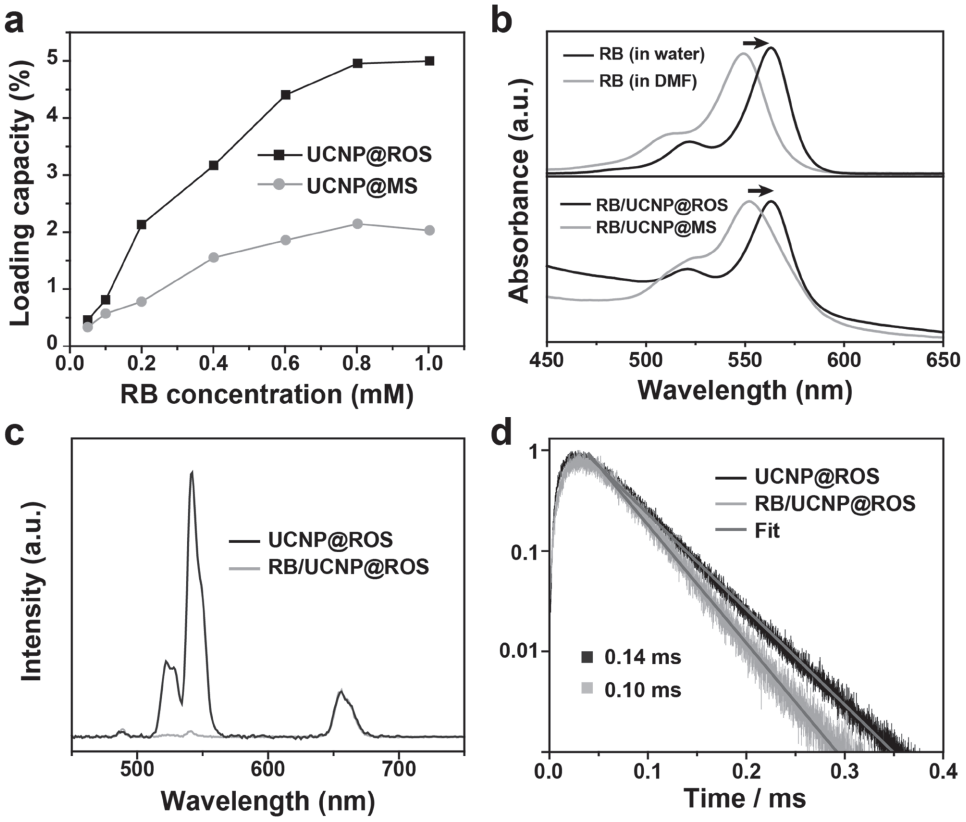

Figure 2. a) RB loading capacity of UCNP@ROS and UCNP@MS at different RB concentration. The capacity was evaluated by the absorbance difference of supernatants after incubation for 24 h. b) Absorbance spectra of RB free RB dispersed in water or DMF (upper panel) and RB loaded in UCNP@ROS or UCNP@MS (lower panel). c) Upconversion fluorescent spectra of UCNP@ROS and RB/UCNP@ROS. The green emission of UCNP@ROS was extremely quenched after RB loading. d) Fluorescence lifetime decay curves of UCNP@ROS and RB/UCNP@ROS monitored at 542 nm (λ_{ex} = 980 nm). The lifetime is calculated by fitting the decay curve with a single exponential function.

Using thioflavin T (ThT) assay, we further verified that the hindrance effect of RB/UCNP@ROS correlates with NIR light illumination time and intensity. ThT, the commonly used dye for evaluating the degree of amyloid aggregation, exhibits an enhanced fluorescence upon its binding to the β-sheet-rich amyloid fibril.[30] As shown in Figure S10 (Supporting Information), ThT fluorescence at 485 nm was reduced accordingly with the increasing illumination time and power density of NIR light. Note that either free RB or bare UCNP@ROS exhibited no appreciable efficacy under NIR light (Figure S11, Supporting Information). Moreover, RB/UCNP@ROS exhibited enhanced inhibitory activity than RB/UCNP@MS which showed low loading capacity and RB disaggregation (Figure S12, Supporting Information). We studied the kinetics of Aβ fibrillation in the presence of NIR-sensitized RB/UCNP@ROS using ThT assay. As shown in Figure 3b, the time required to reach the half maximum of ThT fluorescence (T_{50}) for Aβ samples incubated under dark or NIR light were 5.15 and 5.02 h, respectively, which indicates that NIR light alone does not influence Aβ aggregation kinetics. With RB/UCNP@ROS under dark, a T_{50} of 14.91 h was observed without any noticeable change of the maximum fluorescence intensity. This result implies a decreased elongation rate but unchanged amount of total Aβ aggregates, which is consistent with the decreased length of Aβ fibrils according to the AFM result (Figure 3e). The low elongation rate is attributed to electrostatic binding of Aβ peptides with positively charged amine groups of organosilica shell of UCNP@ROS nanoparticles.[31] Note that six negatively charged residues and three positively charged residues exist in an Aβ peptide, making its net charge of –3. We confirmed the adsorption of Aβ on the nanoparticle surface by the increased particle diameter and the change of surface charge after incubation with Aβ (Figure S7, Supporting Information). We further explored the intrinsic effect of RB/UCNP@ROS on Aβ aggregation. Figure S13 (Supporting Information) shows that Aβ aggregation under dark was retarded when nanocomposite concentration was high (above 100 μg mL^{-1}), while the aggregation was promoted at lower concentration of RB/UCNP@ROS. This result is in a good agreement with the previous studies,[32,33] which reported that the ratio between peptides and nanoparticles plays an important role on the aggregation kinetics.

Upon illumination of NIR light, RB/UCNP@ROS induced not only an increase in T_{50} value to 23.15 h, but also a significant decrease of the maximum ThT fluorescence by 71.5%. We attribute the NIR-induced suppression of Aβ aggregation by RB/UCNP@ROS to localized oxidative stress generated by the photosensitization of RB. According to the literature, the sulfoxidation of methionine 35, which is the most susceptible amino acid to reactive oxygen species, leads to the reduction of assembly of

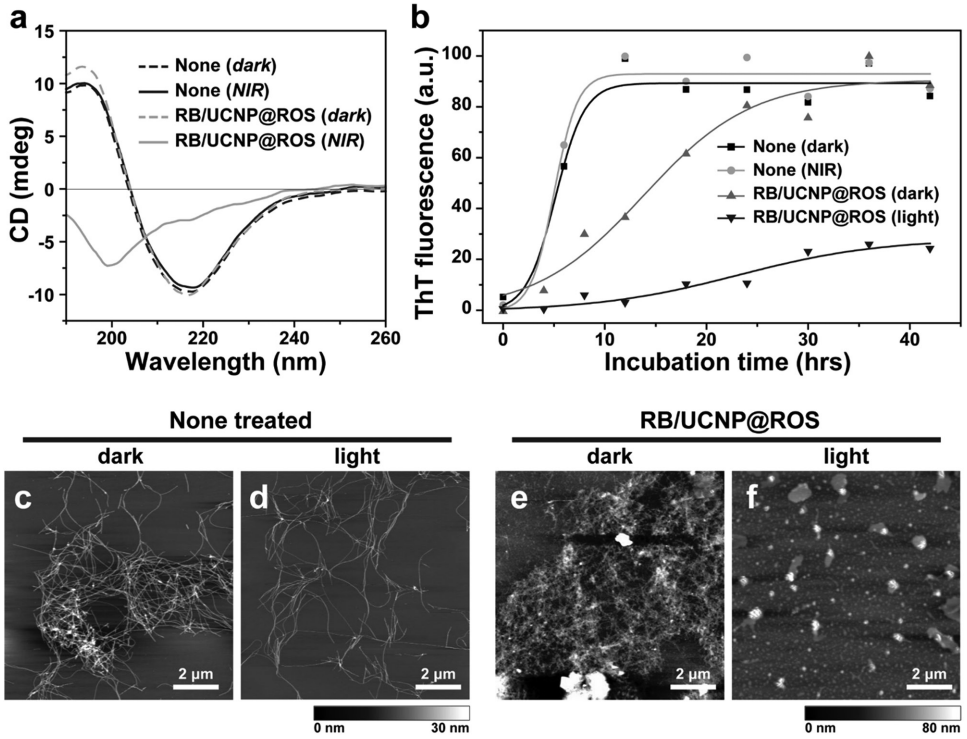

Figure 3. a) Analysis of NIR-mediated inhibition on Aβ aggregation using CD spectroscopy. The CD spectrum shows that two representative peaks of β-sheet structure (195 and 216 nm) completely disappeared with the RB/UCNP@ROS treatment and NIR illumination. The Aβ samples were incubated for 12 h under 980 nm NIR illumination (0.6 W cm^{-2}) and for another 12 h under dark condition. b) The kinetics of Aβ aggregation under various conditions. ThT fluorescence was recorded at 485 nm (λ_{ex} = 440 nm) for 42 h. Ex situ AFM images of Aβ aggregates incubated under c) dark and d) NIR light in the absence of RB/UCNP@ROS treatment and Aβ incubated with RB/UCNP@ROS in the e) dark and f) light.

Aβ peptide by inducing structural and dynamical change of the peptide.[34,35] Upon absorption of visible light energy, RB undergoes a photosensitization reaction and produces $^1O_2$ by transferring its energy to ground-state oxygen molecules.[28] According to our analysis using singlet oxygen sensor green (SOSG) reagent that exhibits fluorescence at 525 nm in the presence of $^1O_2$, neither free RB nor UCNP@ROS generated $^1O_2$ upon 980 nm NIR excitation (Figure S14, Supporting Information). In contrast, RB/UCNP@ROS produced a significant amount of $^1O_2$ under NIR light illumination. This result is consistent with the ThT assay result, showing negligible efficacy of free RB and UCNP@ROS under NIR light (Figure S11, Supporting Information). We also observed the degree of the inhibition under anaerobic conditions (i.e., Ar-saturated buffer containing NaN_3) where $^1O_2$ generation was extremely suppressed. As shown in Figure S15 (Supporting Information), the inhibitory effect of NIR-excited RB/UCNP@ROS on Aβ aggregation in the absence of oxygen was significantly reduced compared to aerobic conditions. To investigate possible oxidative damage of Aβ by NIR-excited RB/UCNP@ROS, we performed 2,4-dinitrophenylhydrazine (DNPH) assay, in which DNPH reacts with carbonyl groups in oxidized proteins and produces hydrazones that exhibit strong absorbance at 360 nm.[36] The result shows that the carbonyl contents in Aβ notably increased after its incubation with RB/UCNP@ROS under NIR light (Figure S16, Supporting Information). Taken together, Aβ peptides bound to the organosilica shell are irreversibly oxidized by $^1O_2$ when NIR light is irradiated. Further studies are needed to minimize cellular toxicity of $^1O_2$ generated from photoexcited RB/UCNP@ROS while maintaining the efficacy of Aβ inhibition. For example, considering that $^1O_2$ has a very short lifetime and only acts close to its generation site,[37] Aβ-specific targeting may minimize cell damage by limiting the location of $^1O_2$ generation. Recently, a number of researchers developed nanoparticles that can selectively bind to Aβ through surface functionalization.[38]

We further investigated whether NIR-excited RB/UCNP@ROS can reduce Aβ-induced cytotoxicity using a pheochromocytoma (PC12) cell model and a 3-(4,5-dimethylthiazol-2yl)-2,5-diphenyltetrazolium bromide (MTT) assay. We confirmed that RB/UCNP@ROS itself is biocompatible; the nanoparticle was not toxic in the broad concentration range from 62.5 μg mL^{-1} to 2 mg mL^{-1} (**Figure 4**a). Aβ peptides incubated for 24 h caused MTT activity to significantly decrease to 57% (Figure 4b), indicating high toxicity of Aβ aggregates to PC12 cells. In contrast, over 97% of cells survived when the neuronal cells were incubated with the Aβ solution treated with NIR-sensitized RB/UCNP@ROS. Note that RB/UCNP@ROS under dark condition did not reduce any Aβ-aggregate-caused cytotoxicity. These results show that the photosensitization of RB/UCNP@ROS by NIR light is effective, not only for blocking Aβ aggregation but also for suppressing the toxicity induced by Aβ aggregates. In addition, statistical analysis conducted by a previous study suggested that UCNP@ROS exhibits a substantial degree of cellular uptake by human embryo lung fibroblasts,[27] which

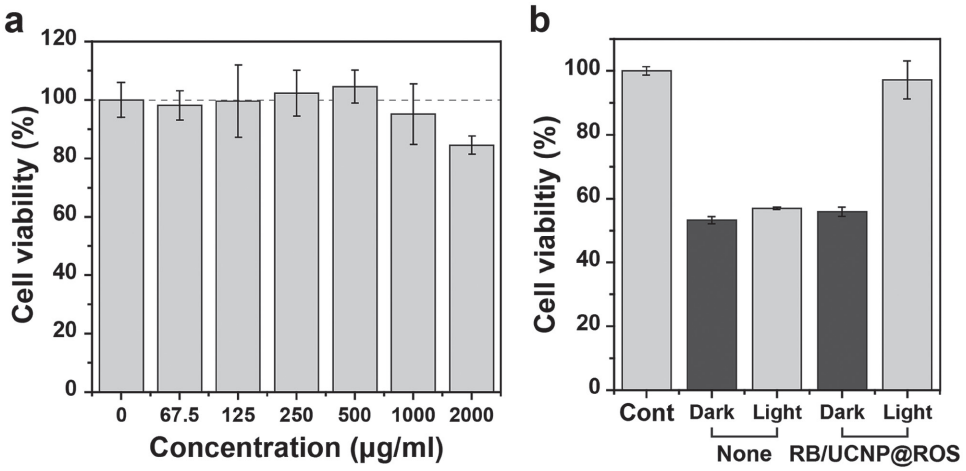

Figure 4. a) Cytotoxicity assay of PC12 cells incubated with RB/UCNP@ROS at various concentrations (0, 67.5, 125, 250, 500, 1000, and 2000 μg mL^{-1}) using MTT assay. UCNP@ROS induced negligible degree of cytotoxicity up to 2 mg mL^{-1}. b) Cell viability of PC12 incubated in the absence or presence of RB/UCNP@ROS treatment with or without NIR light (0.6 W cm^{-2}). ($n \geq 3$, ***$p < 0.001$.) (0.25 mg mL^{-1} UCNP@ROS-RB.) Statistical analysis was carried out by means of one-way analysis of variance (ANOVA).

implies the potential of the nanocomposite as a subcellular therapeutic agent.

In summary, RB-loaded core/shell upconverting nanoparticles effectively suppress Aβ aggregation and toxicity through photosensitization by NIR light. The upconverting nanoparticles with an ROS shell and a $NaYF_4$:Yb,Er core exhibited high energy transfer efficiency to the loaded RB under NIR light illumination, which was derived from a considerable spectral overlap between upconversion emission and RB absorbance, high loading capacity, and low self-aggregation of RB. The RB/UCNP@ROS effectively inhibited the self-assembly of Aβ to aggregates under 980 nm NIR light. We attribute the inhibitory result to the synergistic effect of the binding affinity of Aβ to nanoparticles and the photooxidation of the peptide by $^1O_2$ generated from NIR light-induced photosensitization of RB/UCNP@ROS. To elucidate a detailed molecular mechanism underlying the inhibition, further studies are needed using analytical tools such as mass spectrometry and nuclear magnetic resonance. We found that RB/UCNP@ROS is not only biocompatible but also effective in suppressing the Aβ-induced cytotoxicity under NIR light. Although current study clearly demonstrates the inhibitory effect of RB/UCNP@ROS against Aβ aggregation under NIR light, further studies to investigate its performance in physiological conditions are needed for the medical application. This report, however, suggests a high potential of RB/UCNP@ROS and NIR light in future development of a noninvasive, photodynamic therapy of AD.

Experimental Section

Materials: YCl_3, $YbCl_3$, $ErCl_3$, oleic acid (OA), 1-octadecene (ODE), NaOH, NH_4F, tetraethylorthosilicate (TEOS), 1,4-bis(triethoxysilyl) benzene (BTEB), 3-aminopropyl triethoxysilane (APTES), ammonium hydroxide solution (28%), Igepal CO-520, dicyandiamide, ammonium chloride, rose bengal, hexafluoro-2-propanol, thioflavin T, DNPH, and MTT were purchased from Sigma-Aldrich Chemical Co. (St Louis, MO). Human Aβ_{42} peptide was obtained from rPeptide (Bogart, GA) as a lyophilized powder. For in vitro cytotoxicity experiments, RPMI 1640, horse serum (HS), fetal bovine serum (FBS), and antibiotics were purchased from Welgene Inc., Korea.

Synthesis of Rattle-Structured UCNP@ROS: UCNP@ROS was synthesized according to the literature.[27] $NaYF_4$:Yb(18%),Er(2%) UCNPs (10 mg mL^{-1} in cyclohexane) were prepared by thermal decomposition process as previously reported and added in a mixture of Igepal Co-520 (0.5 mL) and cyclohexane (9 mL) followed by stirring for 3 h.[26] Then, ammonium hydroxide solution (0.75 mL, 30%) was added dropwise into the solution and stirred for 0.5 h. After that, TEOS (75 μL) was added into the mixture and stirred for 6 h. A mixture of BTEB (160 μL) and APTES (80 μL) was added and stirred for another 18 h. By the addition of methanol, UCNP@OS particles were precipitated and collected by centrifugation. These particles were washed three times with cyclohexane and ethanol, and they were redispersed in 10 mL deionized water. For preparing UCNP@ROS particles, surface-protected hot water etching method was followed. Briefly, 10 mL of prepared UCNP@OS solution was mixed with 10 mL deionized water of polyvinylpyrrolidone (PVP) (0.2 g, M_w = 40 000) in a 50 mL flask, stirred for 0.5 h, and then heated to 96 °C. After 6 h, the resulting UCNP@ROS particles were collected by centrifugation and washed with ethanol and deionized water several times.

Loading and Releasing of Photosensitizers: UCNP@ROS (1 mg) was mixed with 1 mL of RB solution in DMF (1 mg mL^{-1}) and stirred for 12 h in the dark. RB-loaded UCNP@ROS nanoparticles were collected by centrifugation and washed with ethanol and PBS for several times. The RB loading capacity of UCNP@ROS was measured by the RB absorption at 563 nm. The weight amount of RB-loaded UCNP@ROS was calculated by subtracting the RB weight in the supernatant from the total RB weight. For the leakage test, 2 mg of RB-loaded UCNP@ROS was soaked in 20 mL of PBS for 7 d at 30 °C incubation. The solution was centrifuged and the supernatant was extracted to determine leaked RB in solution from RB-loaded UCNP@ROS by measuring absorption spectra.

Characterization of UCNP@ROS: Powder XRD patterns of the samples were collected on an X-ray diffractometer (D/MAX-RB X-ray Diffractometer, Rigaku Co., Japan) with Cu Kα1 radiation (λ = 1.5418 Å). The morphology of the upconversion nanoparticles was observed with transmission electron microscopy (TEM, JEM-3011, JEOL, Japan) and elemental mapping was performed on a Cs-corrected scanning transmission electron microscope (STEM, JEM-ARM200F, JEOL, Japan). Solid-state ^{13}C and ^{29}Si cross-polarization magic angle NMR spectra were elucidated using a Solid 400 MHz NB NMR spectrometer (Agilent 400 MHz 54 mm NMR DD2, Agilent Technology, USA) at a Larmor frequency of 79.49 MHz. Chemical properties were estimated by FTIR (200, Jasco Inc., Japan). The diameter distribution and ζ-potentials of UCNPs were determined by means of dynamic light scattering (DLS) measurement (Zetasizer Nano ZS, Malvern, UK). N_2 sorption/desorption measurements were performed on BET surface area and porosimetry analyzer at 77 K (ASAP 2020, Micromeritics, USA). UV–vis absorption spectra were measured with UV–vis absorption spectrophotometer (Jasco Inc., Japan). Upconversion emission spectra were collected with 2 W cm^{-2} continuous-wave 980 nm laser diode (Dragon laser, China) equipped spectrofluorophotometer (Shimadzu Inc., Japan). The lifetime decay curves were detected at 542 and 656 nm by a photomultiplier tube (H3177, Hamamatsu), and the temporal profile was measured by a digital oscilloscope. Pulsed 980 and 488 nm laser generated by Nd:YAG laser (GCR-150, 355 nm, pulse width (FWHM) 7 ns) pumped optical parametric oscillator (OPO) was used for upconversion nanoparticle excitation at the nanosecond scale.

Preparation of Monomeric Aβ Solution: Human Aβ_{42} (1 mg) was dissolved in hexafluoro-2-propanol (HFIP) and kept overnight at RT. The solution was distributed in microcentrifuge tubes (1/16 mg aliquots), put into a vacuum desiccator until lyophilized Aβ was obtained and then stored at –20 °C. Aβ monomer was dissolved in 30 µL buffer solution including CH_3CN (300×10^{-6} M), Na_2CO_3 (300×10^{-6} M), and NaOH (250×10^{-3} M), then sonicated for 30 min. The solution was further diluted with a phosphate buffer (8.5×10^{-3} M) containing NaCl (8.5×10^{-3} M), Na_2CO_3 (14×10^{-6} M), NaOH (0.85×10^{-3} M), and acetonitrile (6.0%; final pH 8.0) to a final concentration of 40×10^{-6} M.

Inhibition of Aβ Aggregation under Visible Light Irradiation: A commercial continuous-wave 980 nm NIR laser diode (Dragon laser, China, 2 W cm^{-2}) was used as a light source. The glass vials containing 40×10^{-6} M of Aβ solution were exposed to NIR light (0.6 mW cm^{-2}) for 12 h while they were incubated for 24 h at 30 °C incubation.

AFM Analysis: Incubated Aβ solutions were dropped onto cleaved mica and then allowed to adsorb for 20 min. AFM images were obtained by the instrument (Digital Instruments Inc., USA) in a trapping mode under air using a NCHR silicon cantilever (Nanosensors Inc., Switzerland).

Native Gel Electrophoresis and Silver Staining: Incubated Aβ solutions were added into a loading buffer containing 50×10^{-3} M Tris HCl, pH 6.8, 10% (v/v) glycerol, 1% SDS, 1% β-mercaptoethanol, and 0.01% bromophenol blue, and then they were loaded on 10% Gradi-Gel II gradient gel (Elpis Biotech., Korea). After running, Aβ peptide distribution was visualized by silver staining. A protein electrophoresis kit was purchased from Bio-Rad Co., USA.

ThT Assay: Incubated Aβ solutions and ThT solution were mixed into a phosphate buffer, to a final concentration of 4% (v/v) Aβ solutions and 20×10^{-6} M of ThT solution in a buffer. The fluorescence of ThT at 485 (λ_{ex} = 440 nm) was monitored by spectrofluorophotometer (Shimadzu Inc., Japan).

CD Analysis: Far-UV (190–260 nm) CD spectra were measured using a spectropolarimeter (Jasco Inc., Japan) at 20 °C. Conformational changes of peptides were analyzed at 195 and 215 nm three times under N_2 blowing atmosphere.

Detection of Singlet Oxygen Generation: 100×10^{-6} M of SOSG (Life Technologies, USA) was added to the prepared solution, to 1% (v/v) final concentration. Under NIR light irradiation or without irradiation condition, fluorescence of solutions was measured every 20 min by spectrofluorophotometer (Shimadzu Inc., Japan) at 525 nm.

DNPH Assay: 480 µL of each incubated 40×10^{-6} M Aβ solution in microcentrifuge tubes was precipitated with a trichloroacetic acid (TCA, 20% final concentration) solution for 10 min in an ice bath and then collected by centrifuging (4 min at 14 000 rpm). After that, 500 µL of 10×10^{-3} M DNPH (2 m of HCl only for reagent blanks) was added into each tube for 1 h at RT. Each sample was precipitated by addition of 20% TCA solution and remains were washed three times with 1 mL of ethanol-ethyl acetate (1:1, v/v) solution. Washed samples were redispersed in a guanidine hydrochloride solution (6 m, pH 2.3) for 15 min at 37 °C. Then, the absorbance spectra of samples were measured by a spectrophotometer (Jasco Inc., Japan).

MTT Assay: Rat pheochromocytoma derived PC12 cells (KTCT., Korea) were cultured in RPMI 1640 media with 10% HS, 5% FBS, and 1% antibiotics under 5% CO_2 atmosphere at 37 °C. Cell line was subcultured at least twice a week. 20×10^4 cells mL^{-1} were seeded into 96-well plates and incubated for 24 h to adsorb to the bottom of the wells. 3 µL of preformed Aβ aggregates were added into each well and then coincubated for an additional 24 h. After that, the media containing Aβ aggregates was removed and replaced with a fresh medium containing 10% MTT solution (5 mg mL^{-1} of MTT powder in a phosphate buffer saline). After 3 h incubation, the resulting formazan (purple colored product) absorbance was measured using a Victor 3 microplate reader (PerkinElmer Inc., USA) at 595 nm.

Supporting Information

Supporting Information is available from the Wiley Online Library or from the author.

Acknowledgements

The authors thank Prof. Hyung Min Kim and Heesu Lee of Kookmin University for technical support of fluorescence lifetime decay measurement. This study was supported by the National Research Foundation via the Creative Research Initiative Center (Grant No. NRF-2015R1A3A2066191), Republic of Korea. S. Kuk and B. I. Lee contributed equally to this work.

[1] R. M. Murphy, *Annu. Rev. Biomed. Eng.* **2002**, *4*, 155.
[2] H. A. Pearson, C. Peers, *J. Physiol.* **2006**, *575*, 5.
[3] J. Hardy, D. J. Selkoe, *Science* **2002**, *297*, 353.
[4] S. Salomone, F. Caraci, G. M. Leggio, J. Fedotova, F. Drago, *Br. J. Clin. Pharmacol.* **2012**, *73*, 504.
[5] F. Re, C. Airoldi, C. Zona, M. Masserini, B. La Ferla, N. Quattrocchi, F. Nicotra, *Curr. Med. Chem.* **2010**, *17*, 2990.
[6] S. I. Yoo, M. Yang, J. R. Brender, V. Subramanian, K. Sun, N. E. Joo, S. H. Jeong, A. Ramamoorthy, N. A. Kotov, *Angew. Chem., Int. Ed.* **2011**, *50*, 5110.
[7] M. Li, X. Yang, J. Ren, K. Qu, X. Qu, *Adv. Mater.* **2012**, *24*, 1722.
[8] A. Taniguchi, D. Sasaki, A. Shiohara, T. Iwatsubo, T. Tomita, Y. Sohma, M. Kanai, *Angew. Chem., Int. Ed.* **2014**, *53*, 1382.
[9] J. S. Lee, B. I. Lee, C. B. Park, *Biomaterials* **2015**, *38*, 43.
[10] M. H. Ahmed, T. E. Keyes, J. A. Byrne, *J. Photochem. Photobiol., A* **2013**, *254*, 1.
[11] B. I. Lee, S. Lee, Y. S. Suh, J. S. Lee, A. K. Kim, O. Y. Kwon, K. Yu, C. B. Park, *Angew. Chem., Int. Ed.* **2015**, *54*, 11472.
[12] M. Li, Y. J. Guan, Z. W. Chen, N. Gao, J. S. Ren, K. Dong, X. G. Qu, *Nano Res.* **2016**, *9*, 2411.
[13] Y. J. Chung, B. I. Lee, J. W. Ko, C. B. Park, *Adv. Healthcare Mater.* **2016**, *5*, 1560.
[14] M. Li, C. Xu, J. Ren, E. Wang, X. Qu, *Chem. Commun.* **2013**, *49*, 11394.
[15] J. P. Celli, B. Q. Spring, I. Rizvi, C. L. Evans, K. S. Samkoe, S. Verma, B. W. Pogue, T. Hasan, *Chem. Rev.* **2010**, *110*, 2795.
[16] M. Nyk, R. Kumar, T. Y. Ohulchanskyy, E. J. Bergey, P. N. Prasad, *Nano Lett.* **2008**, *8*, 3834.
[17] P. Zhang, W. Steelant, M. Kumar, M. Scholfield, *J. Am. Chem. Soc.* **2007**, *129*, 4526.
[18] Q. S. Mei, W. Deng, W. Yisibashaer, H. R. Jing, G. Q. Du, M. Wu, B. N. Li, Y. Zhang, *Small* **2015**, *11*, 4568.
[19] L. Wu, J. S. Wang, M. L. Yin, J. S. Ren, D. Miyoshi, N. Sugimoto, X. G. Qu, *Small* **2014**, *10*, 330.
[20] S. K. Maji, S. Sreejith, J. Joseph, M. J. Lin, T. C. He, Y. Tong, H. D. Sun, S. W. K. Yu, Y. L. Zhao, *Adv. Mater.* **2014**, *26*, 5633.
[21] X. Z. Ai, C. J. H. Ho, J. Aw, A. B. E. Attia, J. Mu, Y. Wang, X. Y. Wang, Y. Wang, X. G. Liu, H. B. Chen, M. Y. Gao, X. Y. Chen, E. K. L. Yeow, G. Liu, M. Olivo, B. G. Xing, *Nat. Commun.* **2016**, *7*, 10432.
[22] S. S. Cui, D. Y. Yin, Y. Q. Chen, Y. F. Di, H. Y. Chen, Y. X. Ma, S. Achilefu, Y. Q. Gu, *ACS Nano* **2013**, *7*, 676.
[23] D. Ni, J. Zhang, W. Bu, H. Xing, F. Han, Q. Xiao, Z. Yao, F. Chen, Q. He, J. Liu, S. Zhang, W. Fan, L. Zhou, W. Peng, J. Shi, *ACS Nano* **2014**, *8*, 1231.
[24] F. Zhou, B. Zheng, Y. Zhang, Y. Wu, H. Wang, J. Chang, *Nanotechnology* **2016**, *27*, 235601.
[25] N. M. Idris, M. K. Gnanasammandhan, J. Zhang, P. C. Ho, R. Mahendran, Y. Zhang, *Nat. Med.* **2012**, *18*, 1580.
[26] J. S. Lee, D. H. Nam, S. K. Kuk, C. B. Park, *Chem. -Eur. J.* **2014**, *20*, 3584.
[27] S. Lu, D. Tu, P. Hu, J. Xu, R. Li, M. Wang, Z. Chen, M. Huang, X. Chen, *Angew. Chem., Int. Ed.* **2015**, *54*, 7915.
[28] M. C. DeRosa, R. J. Crutchley, *Coord. Chem. Rev.* **2002**, *233*, 351.
[29] C. J. Barrow, M. G. Zagorski, *Science* **1991**, *253*, 179.
[30] R. Khurana, C. Coleman, C. Ionescu-Zanetti, S. A. Carter, V. Krishna, R. K. Grover, R. Roy, S. Singh, *J. Struct. Biol.* **2005**, *151*, 229.
[31] Y. Kim, J. H. Park, H. Lee, J. M. Nam, *Sci. Rep.* **2016**, *6*.
[32] S. Radic, T. P. Davis, P. C. Ke, F. Ding, *RSC Adv.* **2015**, *5*, 105498.
[33] R. Vacha, S. Linse, M. Lund, *J. Am. Chem. Soc.* **2014**, *136*, 11776.
[34] L. Hou, I. Kang, R. E. Marchant, M. G. Zagorski, *J. Biol. Chem.* **2002**, *277*, 40173.
[35] Y. Yan, S. A. McCallum, C. Wang, *J. Am. Chem. Soc.* **2008**, *130*, 5394.
[36] R. L. Levine, D. Garland, C. N. Oliver, A. Amici, I. Climent, A. G. Lenz, B. W. Ahn, S. Shaltiel, E. R. Stadtman, *Methods Enzymol.* **1990**, *186*, 464.
[37] A. P. Castano, T. N. Demidova, M. R. Hamblin, *Photodiagn. Photodyn. Ther.* **2004**, *1*, 279.
[38] N. Xiong, X. Y. Dong, J. Zheng, F. F. Liu, Y. Sun, *ACS Appl. Mater. Interfaces* **2015**, *7*, 5650.

Received: September 19, 2016
Revised: November 8, 2016
Published online: January 16, 2017

